Examining the behaviour of PKS 1424-418 during flaring

Pfesesani van Zyl[1,2], Michael Gaylard[1] and Sergio Colafrancesco[2]

[1]Hartebeesthoek Radio Astronomy Observatory, Farm 502JQ, Broederstroom road, Krugersdorp, 1740

[2]WITS School of Physics, 1 Jan Smuts Avenue, Braamfontein, Johannesburg, 2000

E-mail: pfesesani@hartrao.ac.za, mike@hartrao.ac.za, sergio.colafrancesco@wits.ac.za

Abstract. The Fermi Large Area Telescope (Fermi-LAT) is a gamma-ray (γ-ray) telescope designed to observe high energy (HE) γ-ray events with energies between 20 MeV to just over 300 GeV. In October 2012, Fermi-LAT observed an energetic flare from the blazar source PKS 1424-418 reaching an average daily flux of 1.4 $\pm$ 0.2 x 10^{-6} ph cm^{-2}s^{-1}. A flare is considered as This event triggered radio follow up observations with the Hartebeesthoek Radio Astronomy Observatory (HartRAO) 26 m radio telescope. The source was observed at frequencies between 2.3 GHz and 12.2 GHz using the drift scan technique. Soon after the follow up campaign began the source showed sharp increases in the radio flux density at all frequencies, with the 8.4 GHz data rising from about 6.1 Jy to 7.0 Jy within a month in January 2013. In this study we investigate the relationship between the γ-rays and the radio emission and search for time-lags using the discrete correlation function (DCF). We also study how the spectral index varied over time during the flaring event at weekly, 2 weekly and 4 weekly epochs. A Lomb-Scargle periodicity search was performed to investigate whether some periodic modulation was present in the γ-ray data. We find that there is a strong γ-ray/radio correlation with the γ-rays leading the radio with exception of one correlation showing the radio leading the γ-rays. An 86 day period was also discovered in the γ-ray data flares.

1. Introduction

Blazars are amongst the brightest known AGN and emit large amounts of energy across the entire electromagnetic spectrum [1]. They are known to exhibit multi-wavelength variability from radio frequencies to γ-rays [2], polarizations (in the radio and optical wavelengths), and show superluminal motion in their jets which are pointed towards the observer. They are traditionally divided into two main groups, BL Lacertae (BL-Lac) and Flat Spectrum Radio Quasars (FSRQ), blazars that show no emission lines or have broad emission lines in their spectra respectively.

The spectral energy distribution (SED) of blazars is characterized by two broad peaks. The first peak, located between the radio and optical frequencies, is thought to be caused by synchrotron emitting particles in the jet. The second peak, located in the high energy γ-ray region, is due to Inverse Compton scattering of relativistically boosted photons. The nature of the particles responsible for the different emissions is still under debate with some suggesting leptons and others hadrons as the main emission particles. This is one of the many reasons multi-wavelength correlation studies are important. They provide a platform for studying the

underlying physics of violent emission regions from the behavior of different components within the blazar jets ([3],[4]).

In this study we observed the source PKS 1424-418. This is an FSRQ that recently underwent a series of flaring events from October 2012 to September 2013. These events were detected by Fermi-LAT with the lowest flare having energies of about 1.4 ± 0.2 x 10^{-6} ph cm^{-2}s^{-1} and the highest reaching 2.3 ± 0.1 x 10^{-6} ph cm^{-2}s^{-1} for E $>$ 100 MeV. The radio emission detected by the HartRAO 26-m telescope shortly after the first flare showed an increased flux density trend at all wavelengths revealing that there might be a connection between the two energy regimes. Using the DCF, we investigated the correlation between the γ-ray light-curve and the radio light curves of the source. We also investigated the relationship between the radio light curves themselves. We further conducted a periodicity search in the γ-ray data to investigate the presence of a possible periodic modulation in the individual flares.

This paper is arranged as follows: Section 2 describes the observations and the data reduction processes, Section 3 describes the data analysis methods applied to the data, and Section 4 discusses the results.

2. Observations & data reduction

This work is based on observations collected by Fermi-LAT and the HartRAO 26-m telescope during the observing epochs October 2012 to September 2013. The Fermi-LAT data was obtained pre-processed in standard flux density units by Roopesh Ojha[1] from the NASA Goddard Space Flight Center, and therefore this paper will only discuss observations done using the HartRAO 26-m telescope.

2.1. HartRAO 26-m observations

Following the Astronomers telegram (ATel) #4494[2], HartRAO 26-m began follow-up observations on PKS 1424-418 from 17 October 2012. We observed PKS 1424-418 with 2.3-GHz (cryogenically cooled) and 12.2-GHz (uncooled) single-beam receivers, and with 4.8-GHz and 8.4-GHz (cryogenically cooled) dual-beam Dicke-switched receivers. The telescope collected radio emission from the source in both left and right circularly polarized orientations using the drift scan technique. During observations, the telescope is parked a little west of the current source position, then as the source "drifts" over the dish due to the earth's rotation it collects radio emission incident on the dish surface. On average, observations consisted of conducting two scans per day with the exception of days when the telescope was used for Very Long Baseline Interferometry (VLBI) observing.

2.2. Data reduction

To get useful flux density estimates of the source, the received emission from the source had to be calibrated against a known calibrator source of unvarying flux density. PKS 1424-418 was calibrated against Hydra A (3C218) using the flux density equation provided by Ott et al. [8]. The Hydra A measured antenna temperature was corrected for pointing errors that can occur during observing due to ground or atmospheric effects by taking scans of the source at the half-power points to the North and South of the source. Each scan was visually inspected for any irregularities that might make it an outlier, through a series of data quality checks. Radio telescopes are highly temperature sensitive instruments and the observations collected can be affected by contributions from their surroundings.

[1] roopesh.ojha@gmail.com

[2] $http://www.astronomerstelegram.org/?read = 4494$

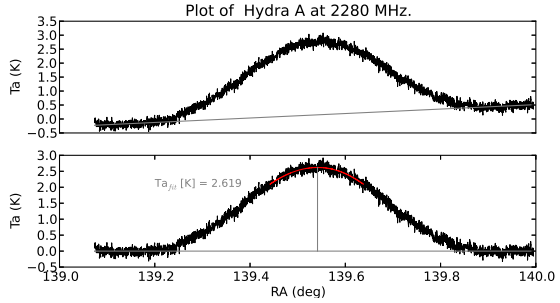

Figure 1. The figure shows two drift scan plots of the source Hydra A. The top figure is the raw drift scan data before reductions. The bottom figure is the raw drift scan after reduction. The red line shows an estimate parabolic peak fit to the top 20% of the data. Ta$_{fit}$ is the maximum antenna temperature for the fit in Kelvins.

2.2.1. Quality checks for outlier detections. As a first step all data containing any one of the following: an RFI (Radio Frequency Interference) signal, step changes in the data (possibly due to receiver instabilities), monotonically increasing data and bumps in the data (due to poor weather conditions that distort the expected bell shaped beam pattern) were considered outliers and removed from observations. These quality checks ensured that all data used in further analysis conformed to the same standard. Under good observing conditions, the system temperature (Tsys) of the observed calibrator source is expected to remain constant throughout the observing campaign. All data scans were examined for deviations in the average Tsys to ensure that none of the elements in the telescope had over-heated during observing. The recorded Tsys per scan had to fall within 2.7 σ of the average Tsys.

3. Data analysis

3.1. Data fitting.

In our second step of the data reduction first order baselines were subtracted from the data to remove any instabilities in the drift scan that may have been caused by the changes in the telescope's surroundings. To find the peak antenna temperature, second order polynomials ($y = ax^2 + bx + c$) were fitted to the top 20% of the scans. Figure 1 shows a typical beam pattern for a drift scan using Hydra A at 2.3 GHz as an example.

3.2. Flux density calculations.

In the last step of our data reduction, we calculated the flux density of the target source using the point source sensitivity (PSS) of the telescope calculated from the calibrator source Hydra A [8]. The calibrator flux density for frequencies < 24 GHz was calculated using,

$$S_{hyd_\nu} = 10exp(0.013 \times log(\nu)^2 - 1.025 \times log(\nu) + 4.729) \qquad [Jy] \tag{1}$$

where S_{hyd_ν} was the Hydra A flux density at a frequency ν. The PSS was calculated separately for each polarization using the equation,

$$PSS = \frac{S_{hyd_\nu}/2}{K_s Ta_{hyd\_pol_\nu}} \qquad [KJy^{-1}] \tag{2}$$

where K_s =1 was the size correction factor and $Ta_{hyd\_pol_\nu}$ was the antenna temperature of the calibrator. The factor of 2 results from the fact that each feed collects half the flux density due to circular polarization. From the PSS, we then calculated the total flux density of the source

(see eq. 3) as the sum of the flux density contributions from the two polarizations. The flux density estimates for each observing day were used to create the light curves in figure 2.

$$S_{src\_pol_\nu}[Jy] = 2 \times PSS_{hyd\_pol_\nu} Ta_{src\_pol_\nu} \tag{3}$$

where $S_{src\_pol_\nu}$ and $Ta_{src\_pol_\nu}$ are the flux density and antenna temperature of the target source PKS 1424-418.

3.3. Correlation analysis

We examined the correlation between γ-rays and radio frequencies using the Discrete Correlation Function (DCF) [9]. The method estimates the time-lag between two discrete light curves. Designed to work with unevenly sampled light curves, the DCF makes no prior assumptions about the data and only calculates the correlation and time-lags for the data sample as is without the interpolation of missing data. Given two light curves x and y, the DCF calculates the cross-correlation function of the light curves using

$$DCF_{ij} = \frac{1}{N}\Big[\sum \frac{(x_i(t) - \bar{x})(y_j(t) - \bar{y})]}{\sqrt{(\sigma_x^2 - e_x^2)(\sigma_y^2 - e_y^2)}}\Big] \tag{4}$$

where $\bar{x}$ and $\bar{y}$ are the means, σ_x and σ_y the standard deviations, and e_x and e_y are the errors of the respective light curves. The DCF estimates an unbinned cross-correlation function for all measured pair points (x_i,y_j), then averages it over a pairwise lag $\Delta t_{ij} = t_j - t_i$ within the range $\tau - \Delta\tau/2 < \Delta\tau < \tau + \Delta\tau/2$ where τ is the time-lag, $\Delta\tau$ is the chosen bin width and N is the number of the unbinned entries. The errors were then estimated as the scatter in the unbinned entries of the DCF terms. We applied Gaussian fits to the top 20% of the peaks to get the lag values in days. The results are shown in Section 4.1. The rapidly varying γ-ray flux density at face value appeared as if it was flaring periodically over time (figure 2). This prompted an investigation into the possible periodicity that might exist within the γ-ray data of the source PKS 1424-418. Periods have been found to exist within γ-ray data [5], but the topic of γ-ray periodicity has been poorly studied and should be approached with caution. The periodicity was analyzed using the period detection method [6], designed for period searches in unevenly sampled data. The significance of the detection was analyzed using the false alarm probability method [7].

4. Results & concluding remarks

Figure 2 displays the 2.3-GHz to 12.2-GHz radio light curves and the γ-ray light curve of the source observed from October 2012 to September 2013. The source shows rapid variability at the higher energies, and a slower more gradual change as you go down in frequency, typical of blazar variability. The 12.2-GHz and 8.4-GHz frequencies showed a steep increase and decrease during the observing period, whereas the 4.8 GHz and 2.3 GHz still showed gradually increasing trends. This is expected as longer wavelengths generally take longer to show variation in their light curves than shorter wavelengths. At 8.4 GHz, there appears to be a sudden upturn towards the end of the light curve, suggesting that something interesting was happening but we require more data to investigate whether this effect was real.

4.1. Correlation

Results from the DCF correlations found that the γ-ray light-curve correlated well with the radio light curves. Table 1 shows a summary of the results obtained for all the correlations. Some DCF correlations were highly scattered especially at longer wavelengths, showing broad peaks and here we give only two examples of the best correlated fits. Figure 3 shows the result

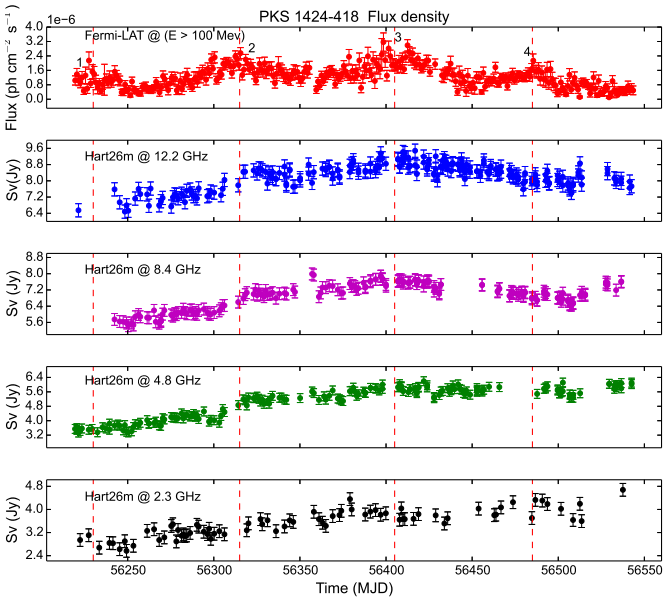

Figure 2. The light curves of observations from both the Fermi-LAT telescope and the HartRAO 26-m radio telescope. The top panel is data collected by Fermi for E > 100 MeV with the flares marked by numbers 1 to 4. The subsequent panels are light curves of data collected by HartRAO 26-m at frequencies 12.2 GHz, 8.4 GHz, 4.8 GHz and 2.3 GHz respectively. The dashed lines indicate the peak flux density epochs of the corresponding flares.

of the γ-ray/12.2-GHz correlation where we found a 23.2 $\pm$ 1.1 day correlation. In this case the γ-rays were leading the radio frequencies as expected. However, figure 4 shows the opposite case with the lower radio frequencies leading the higher radio frequencies for the 12.2-GHz/8.4-GHz correlations, where we found a time-lag of -4.9 $\pm$ 0.6 days. This connection might imply that the HE photons might be relativistically boosted Synchrotron photons, but we need more observations to draw any firm conclusions.

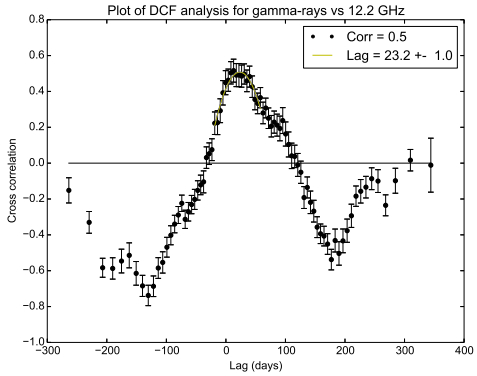

Figure 3. Gamma-rays vs 12.2-GHz light-curve correlation result.

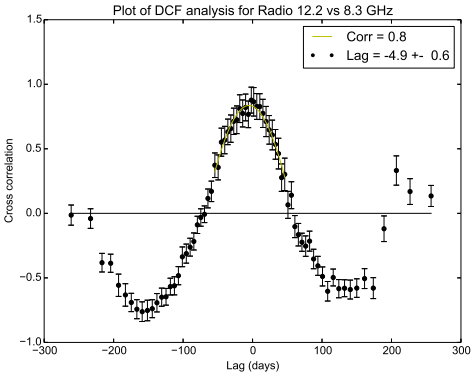

Figure 4. Radio 12.2-GHz vs 8.4-GHz light-curve correlation result.

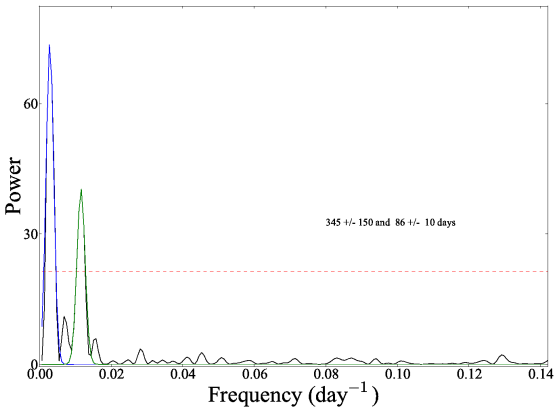

Figure 5. Results for γ-rays/radio and radio/radio DCF correlations. Horizontal line is the 3σ false detection limit.

Light-curve 1	Light-curve 2	Time-lag (days)
γ-rays	12.2 GHz	23.2 $\pm$ 1.0
γ-rays	8.4 GHz	27.9 $\pm$ 1.8
γ-rays	4.8 GHz	68.8 $\pm$ 1.4
γ-rays	2.3 GHz	70.2$\pm$ 2.4
12.2 GHz	8.4 GHz	-4.9 $\pm$ 0.6
12.2 GHz	4.8 GHz	4.8 $\pm$ 1.1
12.2 GHz	2.3 GHz	13.8 $\pm$ 3.1
8.4 GHz	4.8 GHz	3.9 $\pm$ 1.7
8.4 GHz	2.3 GHz	10.4 $\pm$ 2.3
4.8 GHz	2.3 GHz	4.7 $\pm$ 2.9

Table 1. Results for γ-rays/radio and radio/radio DCF correlations.

4.2. Spectral index and periodicity

From the data collected, we also wanted to investigate whether there was a relationship between the variability observed and the spectral index (α), where $S_\nu \sim \nu^\alpha$. We used the two-point spectral index relation $\alpha = \frac{log(S_1/S_2)}{log(\nu_1/\nu_2)}$ where S_1, S_2 and ν_1, ν_2 are the flux density and frequency at two independent radio frequencies respectively. Results obtained showed that there was indeed a relationship between the spectral index and the variability. The spectral index showed increased variability with time between radio light curves that appeared out of phase than those that were in phase during flaring events [10], showing a general trend moving from inverted towards flat. Light curves that appeared in phase e.g. 12.2 and 8.4 GHz, however showed exceptions to the trend by having $\alpha_{12.2-8.4}$ remaining almost constantly inverted over time. The periodicity search produced an 86 $\pm$ 10 day period for the varying flares, the time between two successive local minima, consistent with observations (see figure 4.1).

4.3. Conclusion

From the results it can be seen that in order to investigate the jets in higher detail we would require more observations to provide high cadence light curves. The data suggests that there might be a sharp upturn in the radio at higher frequencies, which could mean that the source was still active in radio long after the γ-rays had reduced to the blazars quiescent stage. From the observations we discovered the source spectrum was inverted due to the flaring, but more importantly we found that there was a γ-ray to radio correlation with the time-lags increasing with wavelength. Results from the spectral index study however suggest that the spectral index hardened after each flare event for light curves in phase, suggesting that each flare event is unique and has its own distinct characteristics. This could be a good indication that splitting each flare and evaluating them separately could prove useful for future studies into multi-variability, see for example [10]. Lastly, the γ-rays produced an 86 $\pm$ 10 day period between flares and a longer 345 $\pm$ 150 day trend for the observing period.

Acknowledgments

This work was jointly supported by the *National Astrophysics and Space Science program* (NASSP) and HartRAO through the *National Research Foundation* (NRF).

References

[1] Urry, C., M., and Padovani, P., 1995, *Publ. Astron. Soc. Pac.*, **107**, 803
[2] Raiteri, C. M., Villata, M., Kadler, M., et al. 2006, aap, **459**, 731
[3] Raiteri, C. M., Villata, M., Smith, P. S., et al. 2012, aap, **545**, AA48
[4] Hovatta, T. H., Tornikoski, M., Lainela, M., et al. 2007, *A&A*, **469**, 899
[5] Nishikawa, D., Hayashi, S., Chamoto, N., et al. 1999 *in Proc. 26th ICRC (Salt Lake City) OG 2.1.17*, **3**, 354
[6] Lomb, N., R., 1976, *Ap&SS*, **39**, 447
[7] Scargle, J., D., 1982 ,*ApJ*, **263**, 835
[8] Ott, M., Witzel, A., Quirrenbach, A., et al. 1994, *A&A*, **284**, 331
[9] Edelson, R., A., and Krolik, J., H., 1988, *ApJ*, **333**, 646
[10] Shabala, S., S., Rogers, J., G., McCallum, J., N., et al. 2014, *Journal of Geodesy*, **88**, 575